

## Last Interglacial peak in mean ocean temperature due to ocean circulation change

Shackleton, S.<sup>1\*</sup>, Baggenstos, D.<sup>2</sup>, Menking, J.A.<sup>3</sup>, Dyonisius, M.N.<sup>4</sup>, Bereiter, B.<sup>2,5</sup>, Bauska,  
 T.K.<sup>6</sup>, Rhodes, R.H.<sup>6</sup>, Brook, E.J.<sup>3</sup>, Petrenko, V.V.<sup>4</sup>, McConnell, J.R.<sup>7</sup>, Kellerhals, T.<sup>2</sup>, Häberli,  
 M.<sup>2</sup>, Schmitt, J.<sup>2</sup>, Fischer, H.<sup>2</sup>, Severinghaus, J.P.<sup>1</sup>

<sup>1</sup>Scripps Institution of Oceanography, University of California, San Diego, La Jolla CA, USA

<sup>2</sup>Climate and Environmental Physics, Physics Institute and Oeschger Center for Climate Change  
 Research, University of Bern, Bern, Switzerland

<sup>3</sup>College of Earth, Ocean, and Atmospheric Sciences, Oregon State University, Corvallis OR,  
 USA

<sup>4</sup>Earth & Environmental Sciences, University of Rochester, Rochester NY, USA

<sup>5</sup>Laboratory for Air Pollution / Environmental Technology, Empa, 8600 Dübendorf, Switzerland

<sup>6</sup>Department of Earth Sciences, University of Cambridge, Cambridge, UK

<sup>7</sup>Division of Hydrologic Sciences, Desert Research Institute, Reno NV, USA

\*Corresponding author: Sarah Shackleton, [sshackle@ucsd.edu](mailto:sshackle@ucsd.edu)

### Abstract

The Last Interglacial (129–116 ka) represents one of the warmest climate intervals of the last  
 800,000 years and the most recent time when sea level was meters higher than today. However, the  
 timing and magnitude of peak warmth varies between reconstructions, and the relative importance of  
 individual sources contributing to elevated sea level (mass gain versus seawater expansion) during the  
 Last Interglacial remains uncertain. Here we present the first mean ocean temperature record for this  
 interval from noble gas measurements in ice cores and constrain the thermal expansion component of  
 sea level. Mean ocean temperature reaches its maximum value of  $1.1 \pm 0.3^\circ\text{C}$  warmer-than-modern at  
 the end of the penultimate deglaciation at 129 ka, resulting in  $0.7 \pm 0.3\text{m}$  of elevated sea level, relative  
 to present. However, this maximum in ocean heat content is a transient feature; mean ocean temperature  
 decreases in the first several thousand years of the interglacial and achieves a stable, comparable-to-  
 modern value by  $\sim 127\text{ ka}$ . The synchronicity of the peak in mean ocean temperature with proxy records  
 of abrupt transitions in oceanic and atmospheric circulation suggests that the mean ocean temperature  
 maximum is related to the accumulation of heat in the ocean interior during the preceding period of  
 reduced overturning circulation.

## 41 Introduction

42 With a heat capacity one thousand times larger than that of the atmosphere, the ocean plays an  
43 important role in regulating the rate and magnitude of global temperature change and represents the  
44 largest energy reservoir in the climate system<sup>1</sup>. Ocean heat uptake and warming contribute directly to  
45 increasing sea level through thermal expansion of seawater and may play a role in future sea level rise  
46 through enhanced sub-shelf melting and subsequent mass loss from the Antarctic Ice Sheet<sup>2</sup>. To  
47 understand the future role of ocean heat uptake, it is instructive to study ocean temperature change  
48 during past warm periods in Earth's history.

49 During the Last Interglacial (LIG, 129-116 ka) surface temperatures were warmer than today,  
50 but existing reconstructions differ substantially on the timing and magnitude of peak warmth. A global  
51 average (land and ocean) surface temperature reconstruction<sup>3</sup> from a compilation of seasonal and  
52 annual-average temperature records shows a maximum of 2°C warmer temperatures during the middle  
53 of the LIG. A global annual-average sea surface temperature (SST) reconstruction<sup>4</sup> shows a maximum  
54 of only 0.5°C warmer-than-preindustrial on a global scale that peaks during the earlier LIG, but up to  
55 1°C warmer in the high latitudes. Climate models show considerable warmth at the mid-LIG, especially  
56 in the high northern latitudes, but in line with the lack of global insolation forcing, little warming or  
57 even cooler conditions on a global scale<sup>5</sup>. At the same time, global sea level during the LIG was 6-9 m  
58 higher<sup>6</sup>. Differences in greenhouse gas and orbital forcing over the LIG relative to modern make the  
59 spatial and temporal patterns of temperature change during this period distinct from what might be  
60 expected from anthropogenic warming<sup>7</sup>. As a result, the LIG is not an analogue for future warming but  
61 offers a unique opportunity to assess the validity of earth system model predictions of sea level rise in  
62 response to warming, provided that reliable paleoclimate data exist for model validation<sup>8</sup>.

63 Sediment cores provide valuable records of changes in ocean conditions through the LIG<sup>4,9-11</sup>  
64 and are critical to understanding the spatiotemporal structure of temperature change. However, because  
65 most available records document surface ocean conditions, deducing total ocean heat content and  
66 thermosteric sea level from these records remains challenging.

67 The measurement of atmospheric noble gases trapped in glacial ice provides a method to  
68 reconstruct changes in mean ocean temperature (MOT) independently from marine records<sup>12-14</sup>.  
69 Changes in the relative atmospheric concentrations of krypton, xenon and nitrogen trace total ocean  
70 heat content because they are caused by temperature-driven changes in gas solubilities in seawater.  
71 Here, we report measurements of the ratios of Kr/N<sub>2</sub>, Xe/N<sub>2</sub>, and Xe/Kr in ice cores from Taylor Glacier  
72 and EPICA Dome C (EDC) ice cores that cover the LIG and penultimate glacial, Marine Isotope Stage  
73 6 (MIS6, 180-136 ka). We assess the timing and magnitude of ocean temperature change during the  
74 LIG and quantify the thermosteric component of elevated sea level during this period.

## **Last Interglacial mean ocean temperature record**

MOT anomalies are calculated relative to the Early Holocene (11– 10 ka) for each ice core because firn fractionation corrections are more robust when calculating relative MOT change compared to absolute MOT values (supplement). MOT anomalies relative to the preindustrial and modern are subsequently calculated using the existing WAIS Divide<sup>12</sup> and EDC<sup>15</sup> Holocene-to-preindustrial MOT records and preindustrial-to-modern simulations of ocean temperature change<sup>16</sup>. Based on Monte Carlo simulations that account for all known sources of uncertainty (methods), we constrain peak MOT to  $1.1 \pm 0.3^\circ\text{C}$  ( $1\sigma$ ) warmer than modern at  $129.0 \pm 0.8$  ka on the Antarctic Ice Core Chronology (AICC2012)<sup>17</sup> (Figure 1). While data for MIS6 and Termination II are relatively sparse, the period of maximum MOT is highly resolved (methods). Because of this and the robust age constraints from trace gas measurements for the Taylor Glacier record (methods/supplement), the timing of peak MOT is well constrained.

The record shows a  $3.4 \pm 0.5^\circ\text{C}$  MOT increase from MIS6 to the early LIG, compared to the LGM to Holocene change of  $2.6 \pm 0.3^\circ\text{C}$ <sup>12</sup>. The larger magnitude in glacial-interglacial MOT change over Termination II versus Termination I is consistent with previous reconstructions of deep ocean temperature during these intervals from stacks of low-resolution marine records<sup>11</sup>.

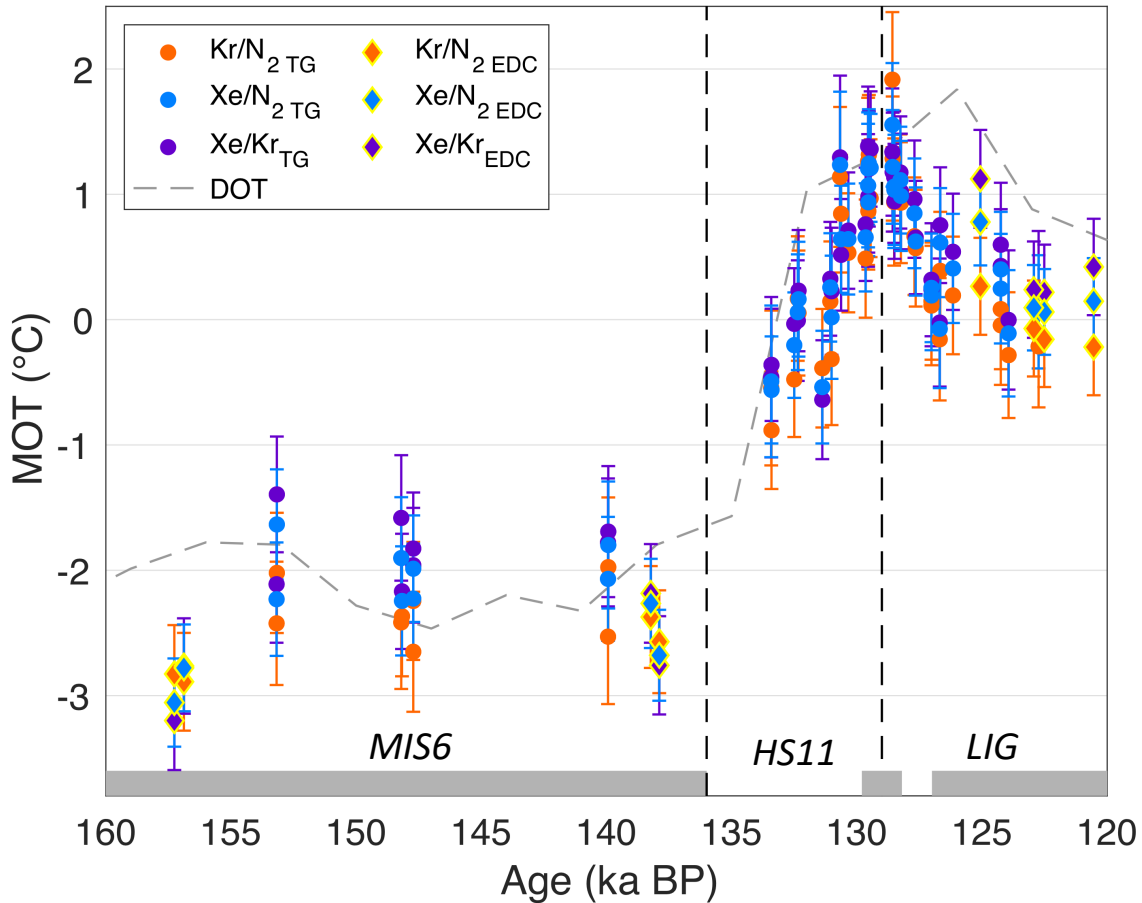


**Figure 1. Mean Ocean Temperature (MOT) anomaly from Kr/N<sub>2</sub>, Xe/N<sub>2</sub>, and Xe/Kr.** MOT data is shown with 1 $\sigma$  error (methods). Vertical dashed lines mark the Marine Isotope Stage 6 (MIS6), Heinrich Stadial 11 (HS11) and Last Interglacial (LIG) boundaries. Gray bars indicate the time intervals for which MIS6 MOT (>136 ka), peak MOT (129.0 $\pm$ 0.8 ka), and stable LIG MOT (<127 ka) are calculated. MOT is reported on the AICC2012<sup>17</sup> chronology. Global average deep ocean temperature (DOT) from stacked marine sediment records<sup>11</sup> on LR04<sup>18</sup> is shown for reference.

### Comparison to global surface temperature records

Comparison of our MOT record to stacked SST records from marine sediments<sup>4</sup> over the LIG reveal distinct differences between these fundamental climate parameters (Figure 2). The maximum in MOT occurs earlier and exceeds the magnitude of the global SST maximum. The magnitude of the peak extratropical SST anomaly agrees well with the peak MOT anomaly, though the temporal evolution of each record over the LIG appears distinct. Comparison of the timing of MOT and SST change is complicated by the lack of absolute age constraints for sediment and ice core records spanning the LIG, and a 1-2 thousand year offset between the SpeleoAge<sup>19</sup> and AICC2012 chronologies that are applied to the SST and MOT records respectively<sup>20</sup>. However,

accounting for the offset in chronologies would actually increase the offset in the relative timing of the MOT and global SST maxima.

While global SST records are good indicators of the ‘skin temperature’ and thus outgoing longwave radiation for much of the planet, MOT is closely related to subsurface heat content<sup>15</sup>. MOT represents volume-averaged ocean temperature, so changes in intermediate and deep ocean temperatures (as opposed to SST changes) play a dominant role in setting MOT. Much of the intermediate and deep ocean’s temperature is set at high latitudes via meridional circulation, so the polar regions are likely crucial for the structure of MOT change, relative to that of global SST<sup>21</sup>.

MOT and Antarctic surface temperature<sup>22</sup> records show strikingly similar features (Figures 2 and 3). Both records are reported on AICC2012, but minor uncertainties in their alignment may result from error in the Taylor Glacier chronology, or the EDC gas-ice age difference<sup>23</sup>. The covariation of MOT and Antarctic temperature during the LIG follows the pattern recently observed during Termination I<sup>12,15</sup> in which mean ocean and high southern latitude surface warming precede the increase in global SST and appear intrinsically linked. We thus have strong evidence that changes in MOT outpace and exceed low latitude SST changes during the LIG, which suggest that polar amplification and intermediate/deep-water formation are key regulators of MOT.

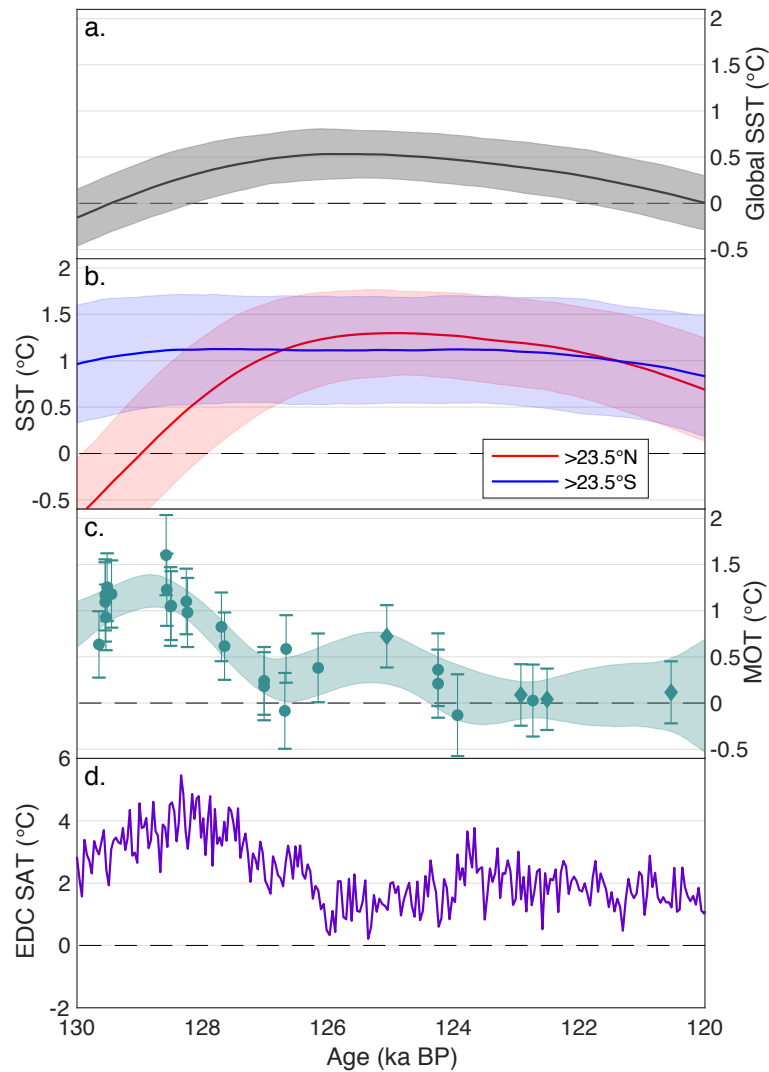


**Figure 2. Surface and mean ocean temperature (MOT) anomalies during the LIG.** **a)** global and **b)** extratropical sea surface temperatures (SST) (relative to preindustrial) from the Northern Hemisphere (red) and Southern Hemisphere (blue) from stacked SST proxy records<sup>4</sup> on the SpeleoAge chronology<sup>19</sup>. Shading shows 2 $\sigma$  confidence interval. **c)** MOT (relative to modern) on AICC2012<sup>17</sup> with 1 $\sigma$  error bars (points) and 1 $\sigma$  confidence envelope (shading). **d)** EPICA Dome C (EDC) surface air temperature<sup>22</sup> (SAT, relative to average of last 1000 years) on AICC2012.

### Links of MOT and ocean circulation over Termination II/LIG

Recent studies have investigated the role of the bipolar seesaw, the out-of-phase temperature variations between hemispheres, in the evolution of glacial terminations<sup>10,19,24,25</sup>. While the exact triggering mechanisms are still debated, it is generally accepted that the bipolar pattern of global temperature anomalies is the result of variations in the strength of the Atlantic Meridional Overturning Circulation (AMOC)<sup>26</sup>. When AMOC is in a strong mode, as today, there is northward

142 heat transport at all latitudes in the Atlantic. When AMOC is weakened, this heat transport is  
143 reduced, leading to a net accumulation of heat in the Southern Hemisphere.

144 A recent synthesis of available high-resolution records covering Termination II<sup>27</sup> including  
145 sediment records from the North Atlantic<sup>10</sup>, Chinese speleothems<sup>25</sup>, and Antarctic ice cores<sup>28,29</sup>  
146 suggest that the AMOC was considerably weakened during Heinrich Stadial 11 (HS11, ~136-129  
147 ka), a cold period in the Northern Hemisphere that covers much of Termination II. At ~129 ka,  
148 these proxy records show a rapid recovery of AMOC and Asian monsoon strength, coinciding with  
149 an abrupt shift in Antarctic moisture source<sup>28</sup>, CH<sub>4</sub> increase<sup>29</sup>, and the peak in MOT in our  
150 reconstruction (Figure 3). Because CH<sub>4</sub> and noble gases are measured on the same ice samples,  
151 there is virtually no uncertainty in the relative timing of the abrupt rise in CH<sub>4</sub> and the MOT  
152 maximum (supplement). The excellent agreement in the timing of peak MOT (129.0±1.9 ka,  
153 including AICC2012 uncertainty) and the end of HS11 (128.9±0.06 ka) dated from the Sanbao  
154 Cave records<sup>25</sup> also suggests an important connection between MOT and the bipolar seesaw.

155 Recent modeling studies have examined the impact of reduced AMOC on surface and  
156 subsurface temperature change through freshwater hosing experiments<sup>14,26,30</sup>. In these simulations,  
157 reduction in AMOC strength results in a globally asymmetric surface pattern of cold Northern  
158 Hemisphere SSTs, as Southern Hemisphere SSTs, MOT, and Antarctica temperatures increase. At  
159 the subsequent recovery of the AMOC, the accumulated subsurface heat is released, leading to an  
160 abrupt increase in Northern Hemisphere SST, and gradual decrease in Southern Hemisphere SST,  
161 Antarctic temperature, and MOT<sup>26</sup>. This spatiotemporal pattern is consistent with the observed  
162 Antarctic temperature and MOT trends during HS11 and the LIG (Figure 3). As in the hosing  
163 simulations, we observe MOT and Antarctic temperature increase during the weakened AMOC  
164 interval of HS11, reach a maximum at ~129 ka synchronous with AMOC recovery<sup>10</sup>, and then  
165 decrease during the several thousand years following AMOC recovery. This mechanism is also  
166 consistent with the lead of Southern Hemisphere over Northern Hemisphere high latitude warming  
167 that is observed at the onset of the LIG<sup>4,9</sup>.

168 These observations raise the question<sup>31</sup> of how much of the warmer-than-modern MOT in  
169 the early LIG was due to the weakened AMOC state, and how much can be attributed to the stable  
170 interglacial climate. In our record, MOT decreased and eventually stabilized by ~127 ka (at latest  
171 by ~124 ka) at a temperature that is comparable to Holocene/modern MOT (+0.2±0.3°C). If the  
172 observed MOT decrease was due to the release of stored heat post-AMOC recovery, then we can  
173 attribute most of the MOT anomaly at the LIG onset to deglacial changes in ocean circulation.

174

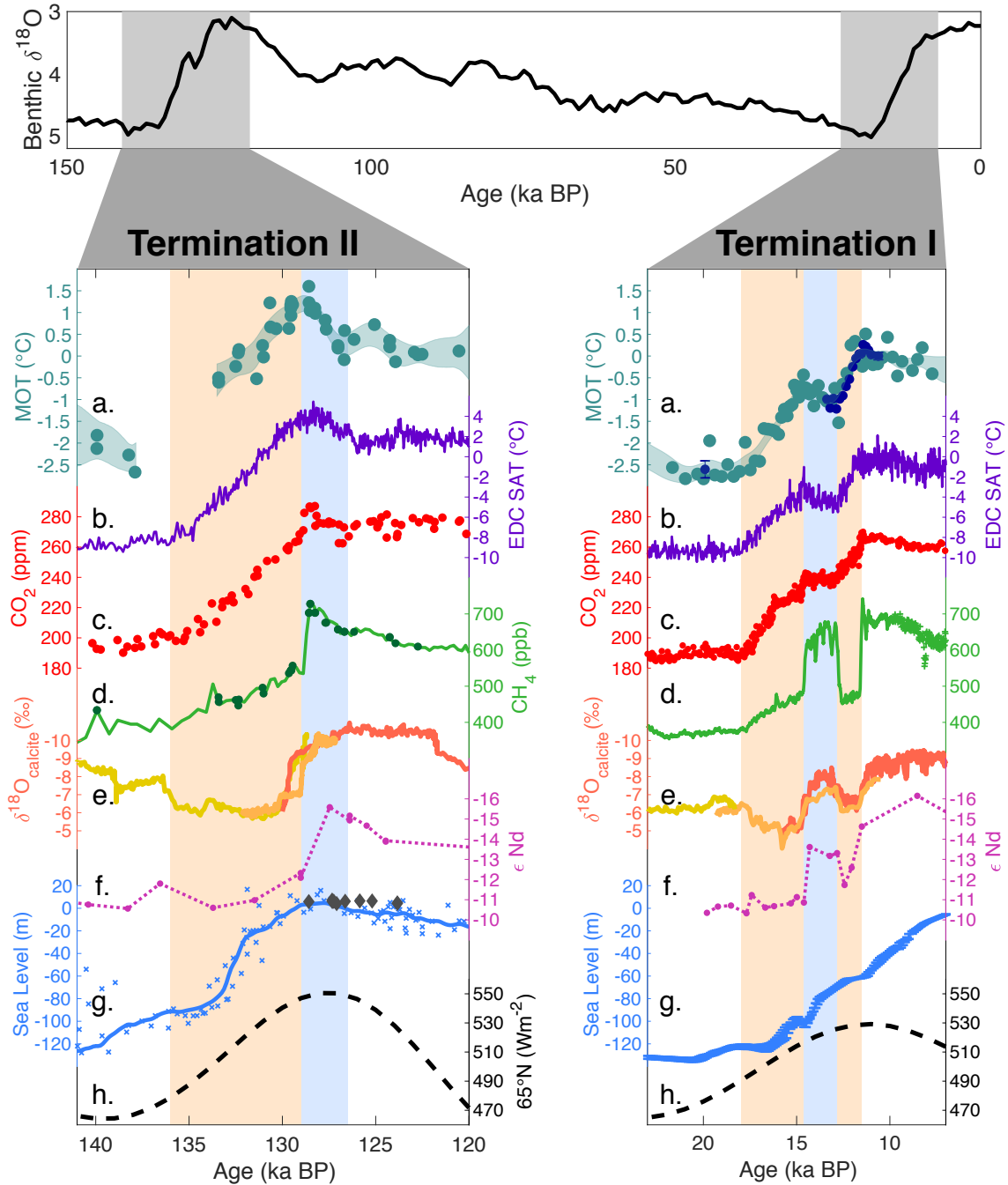


**Figure 3. Climate records of Terminations II and I.** Left panel: climate records of Termination II. **a)** Mean ocean temperature (MOT) anomaly relative to modern from this study with  $1\sigma$  error (shading). **b)** Antarctic temperature<sup>22</sup> anomaly relative to average of last 1000 years, **c)**  $\text{CO}_2$ <sup>32</sup>, and **d)**  $\text{CH}_4$ <sup>29</sup>. Green points show Taylor Glacier  $\text{CH}_4$  measurements. **a)**-**d)** are presented on AICC2012<sup>17</sup>. **e)** Sanbao<sup>25,33</sup>  $^{230}\text{Th}$ -dated  $\delta^{18}\text{O}_{\text{calcite}}$  records. Colors distinguish individual speleothems. **f)** North Atlantic  $\epsilon\text{Nd}$ <sup>10</sup> on core-specific age scale. **g)** Red Sea Level anomaly corrected for isostatic effects<sup>34</sup> on core-specific age scale (light blue). Gray diamonds show coral reef sea level records<sup>35</sup>. **h)** Summer solstice insolation at  $65^\circ\text{N}$ . Right panel: climate records of Termination I with differences



from left panel as follows. **a)** MOT anomaly relative to modern from WAIS Divide<sup>12</sup> (turquoise) and Taylor Glacier<sup>36</sup> (dark blue). Error bars show spread ( $1\sigma$ ) of replicate samples measured at SIO for this study (supplement). **c)** CO<sub>2</sub><sup>37</sup>, and **d)** CH<sub>4</sub><sup>38</sup>. **a)**, **c)** and **d)** are presented on WD2014<sup>39</sup>. **e)** Dongge<sup>40</sup> (red) and Hulu<sup>41</sup> (orange and yellow)  $\delta^{18}\text{O}_{\text{calcite}}$  records. **f)** North Atlantic  $\epsilon\text{Nd}^{42}$  on core-specific age scale **g)** eustatic sea level<sup>43</sup> with  $1\sigma$  error from radiocarbon/uranium-series dated coral and sediment records. Orange bars indicate times when AMOC was in a weakened mode and blue bars show periods of strong AMOC and mean ocean/Antarctic cooling. Top panel: benthic  $\delta^{18}\text{O}$  on LR04<sup>18</sup>. Gray bars highlight the intervals shown in the panels below.

While our Termination II record of MOT lacks resolution at its onset, the only observed warming occurs during the weakened AMOC interval, HS11. Northern Hemisphere insolation forcing during Termination II exceeded that of Termination I, which may in part explain the comparatively rapid disintegration of the Northern Hemisphere ice sheets during Termination II, and long duration of suppressed AMOC due to strong freshwater forcing of the North Atlantic<sup>24</sup>. During Termination I the AMOC temporarily recovered, possibly due to the weaker insolation and thus reduced freshwater forcing<sup>44</sup>. During this time, both Antarctic temperatures and MOT decreased (Figure 3). The so-called ‘Antarctic Cold Reversal’, may in many ways be analogous to the Antarctic and mean ocean cooling observed at the end of Termination II, post-AMOC recovery. While the magnitude of MOT decrease over the Antarctic Cold Reversal was slightly smaller than what is observed for the LIG onset, the net mean ocean warming during Heinrich Stadial I<sup>12</sup> and the Younger Dryas<sup>36</sup> of  $3.4\pm0.4^\circ\text{C}$  is remarkably similar to the net warming found from MIS6 to the LIG peak observed in our record ( $3.4\pm0.5^\circ\text{C}$ ). In addition, the magnitude of glacial-interglacial change across Termination II once MOT has stabilized is  $2.5\pm0.5^\circ\text{C}$ , which is comparable to the magnitude of MOT change across Termination I ( $2.6\pm0.3^\circ\text{C}$ ). Several studies comparing Terminations I and II have posited that the larger magnitude of changes in Antarctic temperature<sup>28</sup> and CO<sub>2</sub><sup>10</sup> across Termination II are related to the delayed recovery of AMOC strength. Our record suggests the same is true for MOT.

These observations suggest that the AMOC interruptions during the past two terminations transiently provided an additional  $\sim 1^\circ\text{C}$  of mean ocean warming above the net glacial-interglacial MOT change. A recent quantitative assessment of Earth’s radiative imbalance over Termination I<sup>15</sup> found maxima in positive radiative imbalance during the Younger Dryas and Heinrich Stadial I, suggesting that reduced AMOC during these intervals contributed energy to the climate system through an increase in ocean heat storage. This storage and subsequent release of energy may play a critical role in terminations<sup>30</sup>. As shown in simulations<sup>30</sup>, when the AMOC is reduced the subsurface ocean works as a ‘capacitor’, storing heat while the surface (centered on the North Atlantic) remains cold. Once the AMOC recovers, the subsurface heat is released, providing

enhanced surface warming. While our MOT record lacks the necessary resolution to conduct a similar assessment of radiative imbalance across Termination II, the comparable magnitudes of enhanced mean ocean warming during weakened AMOC intervals over the last two terminations suggest that this mechanism was also important for Termination II. Along with the potential importance of AMOC interruptions in releasing Southern Ocean CO<sub>2</sub><sup>45,46</sup> and destabilizing Northern Hemisphere ice sheets<sup>47,48</sup>, their role in providing additional energy to the climate system lends support to the hypothesis that AMOC interruptions are not merely incidental to terminations, but play a role in driving the climate out of glacial conditions<sup>19,25</sup>.

### **Implications for West Antarctic Ice Sheet stability**

The MOT changes across the LIG have direct and indirect implications for sea level. Pinning down the sources contributing to the LIG global mean sea level highstand is crucial to understand the vulnerability of modern ice sheets to global warming. From CMIP5 estimates of the expansion efficiency of heat (0.12 m YJ<sup>-1</sup>)<sup>49</sup>, we find that the 1.1±0.3°C MOT anomaly during the early stages of the LIG contributed 0.7±0.3m to elevated sea level. By ~127 ka MOT had decreased to near-modern values, and no appreciable thermosteric contribution (relative to modern) is expected by this early stage in the interglacial. In fact, our record implies a trend of thermosteric sea level lowering in the first several thousand years of the LIG. Coral reef records indicate that sea level was already 5.9±1.7m higher than modern at 128.6±0.8ka<sup>35</sup>, requiring a substantial ice sheet (in addition to the thermosteric) contribution early in the LIG to explain this magnitude of elevated sea level.

The early maximum in MOT may have played another, more indirect role in contributing to sea level rise during the LIG. In recent Antarctic Ice Sheet simulations of the LIG<sup>50,51</sup>, ocean warming played an important role in mass loss from the West Antarctic Ice Sheet. Ref. 50 found that if ocean warming occurred shortly after the glacial termination, the West Antarctic Ice Sheet was more prone to lose mass because of enhanced reverse-sloped beds at grounding lines. By invoking sub-shelf melting through Southern Ocean warming, ref. 51 derived the highest rates of sea level rise during maximum Antarctic temperatures at the end of Termination II, synchronous to our MOT maximum. The delay in AMOC recovery and resulting accumulation of heat in the ocean interior and Southern Hemisphere at the end of Termination II may therefore have played an important role in West Antarctic Ice Sheet mass loss and elevated sea level during the LIG.

An important caveat to consider for this hypothesis is that MOT is not a proxy for ocean temperatures directly under ice shelves, and higher MOT does not necessarily imply that temperatures in vulnerable sub-ice shelf regions were enhanced. However, MOT and the

temperature of circumpolar deep water are intrinsically linked because circumpolar deep water is made up of a representative mixture of waters from all ocean basins<sup>52</sup> and is brought efficiently to the surface by isopycnal mixing in the Southern Ocean. If, as today, circumpolar deep water intruded onto the Antarctic continental shelf, its ice melting capacity would be enhanced during the early stages of the LIG.

## **Conclusions**

The ocean heat anomaly provided from our MOT reconstruction is a simple but important metric to evaluate in earth system models, making it useful for forthcoming simulations of the LIG. Comparison with other proxy and model results suggest that peak MOT coincided with the abrupt recovery of the AMOC at the end of Termination II and was a transient rather than stable feature of the LIG. Enhanced MOT contributed to elevated thermohaline sea level during the early stages of the LIG and may have played a more indirect role in the sea level highstand through amplified melting of ice sheets and shelves from below. The temporal evolution of AMOC and MOT over the past two terminations suggest that the ocean's overturning circulation plays a dominant role in controlling the timing and magnitude of MOT change across terminations; studying the LIG in the context of the termination that preceded it provides a more complete view of the climate evolution that occurred over this interval.

## **Methods**

### **Taylor Glacier sampling and site description**

Taylor Glacier is an outlet glacier of the East Antarctic Ice Sheet with a >80 km long ablation zone exposing easily accessible old ice at the surface. Its accumulation zone is located on the northern flank of Taylor Dome and it terminates in Taylor Valley. Extensive work on mapping the stratigraphy of the glacier identified ice from the LIG located near the terminus of the glacier<sup>53–55</sup>.

For this study, a total of four large-diameter ice cores were collected during the 2014/15 and 2015/16 Antarctic field seasons (Figure S1 in supplement). Two cores spanning approximately 155 – 120 ka were collected approximately 4 km from the glacier terminus. Additionally, two cores were drilled along a previously-established across-flow transect<sup>53</sup> from the early Holocene (10.6 ka) and Last Glacial Maximum (LGM, 19.9 ka) to serve as a comparison to LIG and MIS6 MOT samples. Cores were drilled with the Blue Ice Drill<sup>56</sup> and are 24.1 cm in diameter. Cores were processed and subdivided in the field and analyzed for noble gases for MOT reconstruction as well as other atmospheric gases used to establish the chronology of the record.

### **Taylor Glacier core chronology**

A major challenge in sampling a blue ice area is establishing ages for the samples<sup>57</sup>. Ice from Taylor Glacier has traveled tens of kilometers from its deposition site and has likely undergone non-uniform thinning and folding. While the dynamics of the glacier have been studied

in detail<sup>58,59</sup>, not enough is known about the basal topography or subsurface ice flow to build a chronology for the glacier from a glaciological model.

We therefore use alternative methods to construct the chronology for our samples. Previous work in blue ice areas<sup>53,60–62</sup> has demonstrated success in establishing ice sample chronologies through value and/or inflection point matching of well-mixed atmospheric gases to well-dated ice core records<sup>63</sup>. For this study the chronology was constructed using a least-squares fitting method with measurements of methane concentrations ( $\text{CH}_4$ ), molecular oxygen isotopic composition ( $\delta^{18}\text{O}_{\text{atm}}$ ), and carbon dioxide concentrations ( $\text{CO}_2$ ), tied to EPICA Dome C (EDC) reference records<sup>29,32,64</sup> on the Antarctic Ice Core Chronology (AICC2012)<sup>17,65</sup>. This method allows for a construction of an age probability distribution for each noble gas sample that can be used to assess sample age uncertainty (supplement).

### **Taylor Glacier noble gas measurements**

Taylor Glacier measurements of noble gases for MOT reconstruction were made at Scripps Institution of Oceanography (SIO). A total of 45 ice samples from the 2014/15 and 2015/16 cores were analyzed, including eight replicate samples, giving 37 unique MOT samples. Of the 45 samples, 3 were rejected due to sample age uncertainty (see supplement). In addition, at SIO and Bern five samples from the Holocene (10.6 ka) and five from the LGM (19.9 ka) were measured (Figure 3) at each institution. The motivation for this analysis was to verify the quality of the noble gas records by comparison to published MOT records<sup>12</sup>, and to verify that any offsets in the EDC and Taylor Glacier MOT results were unrelated to lab offsets (see supplementary materials).

The analytical methods for noble gas measurements are described in detail by Bereiter et al. (2018b). In short, ~800 grams of ice were melted under vacuum and liberated gases (~80 ml at standard temperature and pressure, STP) were cryogenically trapped in stainless steel dip tubes. After gas extraction, the samples were split into two aliquots. The larger (~78 ml STP) aliquot was exposed to a Zr/Al alloy at 900°C to remove all non-noble gases and measured on a Thermo-Finnigan MAT-253 isotope ratio mass spectrometer via dual inlet method for  $^{40}\text{Ar}/^{38}\text{Ar}$  ( $\delta^{40/38}\text{Ar}$ ),  $^{40}\text{Ar}/^{36}\text{Ar}$  ( $\delta^{40/36}\text{Ar}$ ),  $^{86}\text{Kr}/^{84}\text{Kr}$  ( $\delta^{86/84}\text{Kr}$ ),  $^{86}\text{Kr}/^{83}\text{Kr}$  ( $\delta^{86/83}\text{Kr}$ ),  $^{86}\text{Kr}/^{82}\text{Kr}$  ( $\delta^{86/82}\text{Kr}$ ),  $^{84}\text{Kr}/^{40}\text{Ar}$  ( $\delta\text{Kr}/\text{Ar}$ ), and  $^{132}\text{Xe}/^{40}\text{Ar}$  ( $\delta\text{Xe}/\text{Ar}$ ). The smaller aliquot (~2 ml, STP) was passed through a cryotrap (-196°C) to remove  $\text{CO}_2$  and measured on a Thermo-Finnigan MAT Delta V isotope ratio mass spectrometer via dual inlet method for  $^{29}\text{N}_2/^{28}\text{N}_2$  ( $\delta^{15}\text{N}$ ),  $^{34}\text{O}_2/^{32}\text{O}_2$  ( $\delta^{18}\text{O}$ ),  $^{32}\text{O}_2/^{28}\text{N}_2$  ( $\delta\text{O}_2/\text{N}_2$ ), and  $^{40}\text{Ar}/^{28}\text{N}_2$  ( $\delta\text{Ar}/\text{N}_2$ ). Measurements were corrected for pressure imbalance and chemical slope according to established procedure<sup>67</sup>.

All data are reported in delta notation, relative to a modern atmosphere standard. Because argon is preferentially lost relative to xenon and krypton during ice bubble formation<sup>68</sup>, we mathematically combine  $\delta\text{Xe}/\text{Ar}$ ,  $\delta\text{Kr}/\text{Ar}$ , and  $\delta\text{Ar}/\text{N}_2$  to obtain  $\delta\text{Kr}/\text{N}_2$ ,  $\delta\text{Xe}/\text{N}_2$ , and  $\delta\text{Xe}/\text{Kr}$ .

### **Taylor Glacier fractionation corrections**

To reconstruct ocean temperature from  $\text{Kr}/\text{N}_2$ ,  $\text{Xe}/\text{N}_2$  and  $\text{Xe}/\text{Kr}$ , it is necessary to correct for fractionation during firnification, the process by which fresh snow compacts, transitioning to denser firn and eventually to glacial ice containing air trapped in bubbles. While the free troposphere is well mixed through convective processes, the low permeability of the firn restricts bulk flow; gases within the firn column are transported primarily via molecular diffusion<sup>69</sup>. This allows for gravitational settling and thermal diffusion to alter firn air from its atmospheric composition before it is occluded in glacial ice<sup>70,71</sup>. As such,  $\text{Kr}/\text{N}_2$ ,  $\text{Xe}/\text{N}_2$  and  $\text{Xe}/\text{Kr}$  must be corrected for fractionating processes to derive the paleoatmospheric composition for inferring MOT.

As suggested by ref. 12, under/over-correction of fractionation may lead to systematic offsets in MOT, but the effect primarily impacts the absolute MOT anomaly (relative to modern) and has little impact on relative MOT change within a record. We investigate the influence of the choice in methods of fractionation correction on the MOT record and find that different methods shift the absolute MOT record up or down but have little effect on relative MOT change in the Taylor Glacier record (see supplement). We thus compute the MOT anomalies relative to the Taylor Glacier Holocene (10.6 ka) samples and then estimate the Holocene – modern MOT difference (and uncertainties) from the WAIS Divide MOT record and model simulations of ocean heat content over the last 2000 years<sup>16</sup>. A detailed description and assessment of the fractionation corrections is included in the supplementary materials.

### **EDC ice core noble gas analysis**

Four EDC ice core samples from the LIG and four from MIS6 were analyzed at the University of Bern and included in this study. Measurement and data processing for these samples are similar to the analysis of Taylor Glacier samples with a few important distinctions (ref. 15 and supplement). Chronological uncertainties are not considered in this analysis, because the Taylor Glacier chronology is tied to that of EDC through ice core synchronization and contribute minimally to the total uncertainty for these samples. In addition, the approach to firn fractionation corrections differs slightly between Taylor Glacier and EDC (supplementary section SI4).

### **Derivation of MOT from noble gas data**

To reconstruct MOT values from fractionation-corrected Kr/N<sub>2</sub>, Xe/N<sub>2</sub> and Xe/Kr, we use the ocean-atmosphere box model of ref. 12 with several modifications. We make no assumptions about the glacial-interglacial change in the ocean saturation state and use current estimates of krypton and xenon undersaturation<sup>72</sup> in the box model for the entirety of the record. We also do not invoke the glacial-interglacial changes in the relative water mass distributions that were applied in ref. 12 and use the modern distributions of Antarctic Bottom Water and North Atlantic Deep Water to derive MOT over the full record.

We account for the effects of changes in ocean salinity, volume, and atmospheric pressure on the oceanic inventories of krypton, xenon and nitrogen using the sea level record of ref. 34 corrected for isostatic effects (supplement). We also include the influence of the large ice shelf over the Arctic during MIS6, which holds the equivalent of 15 meters of sea level, influencing ocean salinity and volume, but not sea level<sup>73</sup>.

To assess uncertainty in our MOT record we run 10,000 Monte Carlo simulations of our reconstruction with all known analytical and dating uncertainties in the MOT and sea level records, as well as the uncertainty in the Holocene-to-modern MOT change. We include uncertainties in measured Kr/N<sub>2</sub>, Xe/N<sub>2</sub> and Xe/Kr and the isotope data used to correct for firn processes in our simulations, as well as the method used for fractionation corrections (supplementary section SI4). To account for age uncertainties in the MOT record, we use an inverse transform method<sup>74</sup> to randomly sample from our age probability distribution to include in our Monte Carlo simulations. For our final uncertainty estimate, we use the average of the three MOT records (and the Monte Carlo simulations) from Kr/N<sub>2</sub>, Xe/N<sub>2</sub> and Xe/Kr to minimize the influence of analytical noise from any single measurement.

The 1 $\sigma$  confidence envelope shown in Figures 2 and 3 was constructed using the MATLAB cubic smoothing spline function (csaps) with a 2500 year cut off period on the 10,000 Monte Carlo MOT reconstructions. Each reconstruction was resampled using a bootstrapping method before the spline was produced. The 1 $\sigma$  confidence envelope was then calculated from the distribution of the Monte Carlo splines at each time interval in the record.

## Data availability

Presented data are available online at (\*\*\*\*\*).

## References

1. Stocker, T. F. *et al.* Climate change 2013: The physical science basis. (2013).
2. Pritchard, H. D. *et al.* Antarctic ice-sheet loss driven by basal melting of ice shelves. *Nature* **484**, 502–505 (2012).
3. Snyder, C. W. Evolution of global temperature over the past two million years. *Nature* **538**, 226–228 (2016).
4. Hoffman, J. S., Parnell, A. C. & He, F. Regional and global sea-surface temperatures during the last interglaciation. *Science* **279**, 276–279 (2017).
5. Otto-Bliesner, B. L. *et al.* How warm was the last interglacial? New model – data comparisons. *Philos. Trans. R. Soc. A* **371**, (2013).
6. Kopp, R. E., Simons, F. J., Mitrovica, J. X., Maloof, A. C. & Oppenheimer, M. Probabilistic assessment of sea level during the last interglacial stage. *Nature* **462**, 863–867 (2009).
7. Masson-Delmotte, V. *et al.* Sensitivity of interglacial Greenland temperature and  $\delta^{18}\text{O}$ : ice core data, orbital and increased  $\text{CO}_2$  climate simulations. *Clim. Past* **7**, 1041–1059 (2011).
8. Fischer, H. *et al.* Palaeoclimate constraints on the impact of 2°C anthropogenic warming and beyond. *Nat. Geosci.* **11**, 475–485 (2018).
9. Capron, E. *et al.* Temporal and spatial structure of multi-millennial temperature changes at high latitudes during the Last Interglacial. *Quat. Sci. Rev.* **103**, 116–133 (2014).
10. Deaney, E. L., Barker, S. & Flierdt, T. Van De. Timing and nature of AMOC recovery across Termination 2 and magnitude of deglacial  $\text{CO}_2$  change. *Nat. Commun.* **8**, 1–10 (2017).
11. Shakun, J. D., Lea, D. W., Lisiecki, L. E. & Raymo, M. E. An 800-kyr record of global surface ocean  $\delta^{18}\text{O}$  and implications for ice volume-temperature coupling. *Earth Planet. Sci. Lett.* **426**, 58–68 (2015).
12. Bereiter, B., Shackleton, S., Baggenstos, D., Kawamura, K. & Severinghaus, J. Mean global ocean temperatures during the last glacial transition. *Nature* **553**, 39–44 (2018).
13. Headly, M. A. & Severinghaus, J. P. A method to measure  $\text{Kr}/\text{N}_2$  ratios in air bubbles trapped in ice cores and its application in reconstructing past mean ocean temperature. *J. Geophys. Res.* **112**, 1–12 (2007).
14. Ritz, S. P., Stocker, T. F. & Severinghaus, J. P. Noble gases as proxies of mean ocean temperature : sensitivity studies using a climate model of reduced complexity. *Quat. Sci. Rev.* **30**, 3728–3741 (2011).
15. Baggenstos, D. *et al.* The Earth’s radiative imbalance from the Last Glacial Maximum to the present. *Proc. Natl. Acad. Sci.* **116**, 14881–14886 (2019).
16. Gebbie, G. & Huybers, P. The Little Ice Age and 20th-century deep Pacific cooling. *Science* **363**, 70–74 (2019).
17. Bazin, L. *et al.* An optimized multi-proxy, multi-site Antarctic ice and gas orbital chronology (AICC2012): 120-800 ka. *Clim. Past* **9**, 1715–1731 (2013).
18. Lisiecki, L. E. & Raymo, M. E. A Pliocene-Pleistocene stack of 57 globally distributed benthic  $\delta^{18}\text{O}$  records. *Paleoceanography* **20**, (2005).
19. Barker, S. *et al.* 800,000 Years of Abrupt Climate Variability. *Science* **334**, 347–352 (2011).
20. Capron, E., Govin, A., Feng, R., Otto-Bliesner, B. L. & Wolff, E. W. Critical evaluation of climate syntheses to benchmark CMIP6 / PMIP4 127 ka Last Interglacial simulations in

- the high-latitude regions. *Quat. Sci. Rev.* **168**, 137–150 (2017).
21. Gebbie, G. & Huybers, P. How is the ocean filled ? *Geophys. Res. Lett.* **38**, (2011).
  22. Jouzel, J. *et al.* Orbital and Millennial Antarctic Climate Variability over the Past 800,000 years. *Science* **317**, 793–796 (2007).
  23. Parrenin, F. *et al.* On the gas-ice depth difference ( $\Delta$  depth) along the EPICA Dome C ice core. *Clim. Past* **8**, 1239–1255 (2012).
  24. Marino, G. *et al.* Bipolar seesaw control on last interglacial sea level. *Nature* **522**, 197–201 (2015).
  25. Cheng, H. *et al.* Ice Age Terminations. *Science* **326**, 248–252 (2009).
  26. Pedro, J. B. *et al.* Beyond the bipolar seesaw: Toward a process understanding of interhemispheric coupling. *Quat. Sci. Rev.* **192**, 27–46 (2018).
  27. Menviel, L. *et al.* The penultimate deglaciation: protocol for PMIP4 transient numerical simulations between 140 and 127 ka , version 1.0. *Geosci. Model Dev. Discuss.* (2019).
  28. Masson-Delmotte, V. *et al.* Abrupt change of Antarctic moisture origin at the end of Termination II. *Proc. Natl. Acad. Sci.* **107**, 10–13 (2010).
  29. Loulergue, L. *et al.* Orbital and millennial-scale features of atmospheric CH<sub>4</sub> over the past 800,000 years. *Nature* **453**, 383–386 (2008).
  30. Galbraith, E. D., Merlis, T. M. & Palter, J. B. Destabilization of glacial climate by the radiative impact of Atlantic Meridional Overturning Circulation disruptions. *Geophys. Res. Lett.* **43**, 8214–8221 (2016).
  31. Barker, S. *et al.* Early interglacial legacy of deglacial climate instability. *Paleoceanogr. Paleoclimatology* (2019). doi:10.1029/2019PA003661
  32. Schneider, R., Schmitt, J., Köhler, P., Joos, F. & Fischer, H. A reconstruction of atmospheric carbon dioxide and its stable carbon isotopic composition from the penultimate glacial maximum to the last glacial inception. *Clim. Past* **9**, 2507–2523 (2013).
  33. Wang, Y. *et al.* Millennial- and orbital-scale changes in the East Asian monsoon over the past 224,000 years. *Nature* **451**, 1090–1093 (2008).
  34. Grant, K. M. *et al.* Sea-level variability over five glacial cycles. *Nat. Commun.* **5**, 1–9 (2014).
  35. Dutton, A., Webster, J. M., Zwart, D. & Lambeck, K. Tropical tales of polar ice: evidence of Last Interglacial polar ice sheet retreat recorded by fossil reefs of the granitic Seychelles islands. *Quat. Sci. Rev.* **107**, 182–196 (2015).
  36. Shackleton, S. *et al.* Is the Noble Gas-Based Rate of Ocean Warming During the Younger Dryas Overestimated? *Geophys. Res. Lett.* **46**, (2019).
  37. Marcott, S. A. *et al.* Centennial-scale changes in the global carbon cycle during the last deglaciation. *Nature* **514**, 616–619 (2014).
  38. Buizert, C. *et al.* Precise interglacial phasing of abrupt climate change during the last ice age. *Nature* **520**, 661–665 (2015).
  39. Buizert, C. *et al.* The WAIS-Divide deep ice core WD2014 chronology – Part 1 : Methane synchronization ( 68 – 31 ka BP ) and the gas age-ice age difference. *Clim. Past* **11**, 153 (2015).
  40. Dykoski, C. A. *et al.* A high-resolution, absolute-dated Holocene and deglacial Asian monsoon record from Dongge Cave, China. *Earth Planet. Sci. Lett.* **233**, 71–86 (2005).
  41. Wang, Y. *et al.* A high-resolution absolute-dated late pleistocene monsoon record from Hulu Cave, China. *Science* **294**, 2345–2348 (2001).
  42. Roberts, N. L., Piotrowski, A. M., McManus, J. F. & Keigwin, L. D. Synchronous Deglacial Overturning and Water Mass Source Changes. *Science* **327**, 75–78 (2010).
  43. Lambeck, K., Rouby, H., Purcell, A., Sun, Y. & Sambridge, M. Sea level and global ice volumes from the Last Glacial Maximum to the Holocene. *Proc. Natl. Acad. Sci.* **111**,

- 15296–15303 (2014).
44. Carlson, A. E. Why there was not a Younger Dryas-like event during the Penultimate Deglaciation. *Quat. Sci. Rev.* **27**, 882–887 (2008).
  45. Anderson, R. F. *et al.* Wind-driven upwelling in the southern ocean and the deglacial rise in atmospheric CO<sub>2</sub>. *Science* **323**, 1443–1448 (2009).
  46. Toggweiler, J. R., Russell, J. L. & Carson, S. R. Midlatitude westerlies, atmospheric CO<sub>2</sub>, and climate change during the ice ages. *Paleoceanography* **21**, 1–15 (2006).
  47. Marcott, S. A. *et al.* Ice-shelf collapse from subsurface warming as a trigger for Heinrich events. *Proc. Natl. Acad. Sci.* **108**, 13415 LP – 13419 (2011).
  48. Bassis, J. N., Peterson, S. V & Cathles, L. Mac. Heinrich events triggered by ocean forcing and modulated by isostatic adjustment. *Nature* **542**, 332–334 (2017).
  49. Kuhlbrodt, T. & Gregory, J. M. Ocean heat uptake and its consequences for the magnitude of sea level rise and climate change. *Geophys. Res. Lett.* **39**, 1–6 (2012).
  50. Pollard, D. & Deconto, R. M. Contribution of Antarctica to past and future sea-level rise. *Nature* **531**, 591–597 (2016).
  51. Sutter, J., Gierz, P., Grosfeld, K., Thoma, M. & Lohmann, G. Ocean temperature thresholds for Last Interglacial West Antarctic Ice Sheet collapse. *Geophys. Res. Lett.* **43**, 2675–2682 (2016).
  52. Elderfield, H. *et al.* Evolution of Ocean Temperature and Ice Volume Through the Mid-Pleistocene Climate Transition. *Science* **337**, (2012).
  53. Baggenstos, D. *et al.* Atmospheric gas records from Taylor Glacier, Antarctica, reveal ancient ice with ages spanning the entire last glacial cycle. *Clim. Past* **13**, 943–958 (2017).
  54. Buizert, C. *et al.* Radiometric 81Kr dating identifies 120,000-year-old ice at Taylor Glacier, Antarctica. *Proc. Natl. Acad. Sci.* **111**, 6876–6881 (2014).
  55. Aarons, S. M., Aciego, S. M., McConnell, J. R., Delmonte, B. & Baccolo, G. Dust transport to the Taylor Glacier, Antarctica during the last interglacial. *Geophys. Res. Lett.* **46**, 2261–2270 (2019).
  56. Kuhl, T. W. *et al.* A new large-diameter ice-core drill: The Blue Ice Drill. *Ann. Glaciol.* **55**, 1–6 (2014).
  57. Bintanja, R. On the glaciological, meteorological, and climatological significance of Antarctic blue ice areas. *Rev. Geophys.* **37**, 337–359 (1999).
  58. Aciego, S. M., Cuffey, K. M., Kavanaugh, J. L., Morse, D. L. & Severinghaus, J. P. Pleistocene ice and paleo-strain rates at Taylor Glacier, Antarctica. *Quat. Res.* **68**, 303–313 (2007).
  59. Kavanaugh, J. L. & Cuffey, K. M. Dynamics and mass balance of Taylor Glacier, Antarctica: 2. Force balance and longitudinal coupling. *J. Geophys. Res.* **114**, (2009).
  60. Petrenko, V. V., Severinghaus, J. P., Brook, E. J., Reeh, N. & Schaefer, H. Gas records from the West Greenland ice margin covering the Last Glacial Termination : a horizontal ice core. *Quat. Sci. Rev.* **25**, 865–875 (2006).
  61. Bauska, T. K. *et al.* Carbon isotopes characterize rapid changes in atmospheric carbon dioxide during the last deglaciation. *Proc. Natl. Acad. Sci.* **113**, 3465–3470 (2016).
  62. Menking, J. A. *et al.* Spatial pattern of accumulation at Taylor Dome during Marine Isotope Stage 4 : stratigraphic constraints from Taylor Glacier. *Clim. Past* **15**, 1537–1556 (2019).
  63. Blunier, T. *et al.* Synchronization of ice core records via atmospheric gases. *Clim. Past* **3**, 325–330 (2007).
  64. Landais, A. *et al.* Two-phase change in CO<sub>2</sub>, Antarctic temperature and global climate during Termination II. *Nat. Geosci.* **6**, 1062–1065 (2013).
  65. Veres, D. *et al.* The Antarctic ice core chronology (AICC2012): an optimized for the last 120 thousand years. *Clim. Past* **9**, 1733–1748 (2013).



66. Bereiter, B., Kawamura, K. & Severinghaus, J. P. New methods for measuring atmospheric heavy noble gas isotope and elemental ratios in ice core samples. *Rapid Commun. Mass Spectrom.* **32**, 801–814 (2018).
67. Severinghaus, J. P., Grachev, A., Luz, B. & Caillon, N. A method for precise measurement of argon 40/36 and krypton/argon ratios in trapped air in polar ice with applications to past firn thickness and abrupt climate change in Greenland and at Siple Dome, Antarctica. *Geochim. Cosmochim. Acta* **67**, 325–343 (2003).
68. Severinghaus, J. P. & Battle, M. O. Fractionation of gases in polar ice during bubble close-off: New constraints from firn air Ne, Kr and Xe observations. *Earth Planet. Sci. Lett.* **244**, 474–500 (2006).
69. Schwander, J., Stauffer, B. & Sigg, A. Air mixing in firn and the age of the air at pore close-off. *Ann. Glaciol.* **10**, 141–145 (1988).
70. Schwander, J. The transformation of snow to ice and the occlusion of gases. in *The Environmental Record in Glaciers and Ice Sheets* (eds. Oeschger, H. & Langway, C. C.) 53–67 (1989).
71. Severinghaus, J. P., Sowers, T., Brook, E. J., Alley, R. B. & Bender, M. L. Timing of abrupt climate change at the end of the younger dryas interval from thermally fractionated gases in polar ice. *Nature* **391**, 141–146 (1998).
72. Hamme, R. C. & Severinghaus, J. P. Trace gas disequilibria during deep-water formation. *Deep Sea Res.* **54**, 939–950 (2007).
73. Nilsson, J. *et al.* Ice-shelf damming in the glacial Arctic Ocean : dynamical regimes of a basin-covering kilometre-thick ice shelf. *Cryosph.* **11**, 1745–1765 (2017).
74. Kolmogorov, A. N. *Foundations of the Theory of Probability*. (Chelsea Publishing Company, 1950).

#### Corresponding Author

Correspondence and request for materials should be addressed to S.S. at sshackle@ucsd.edu.

#### Acknowledgements

This research was supported by NSF grants 1246148 (SIO), 1245821 (OSU) and 1245659 (UR). We thank Kathy Schroeder, Mike Jayred, Peter Sperlich, Isaac Vimont, Jacob Ward, Heidi Roop, Peter Neff, and Andrew Smith for their invaluable field support for this project. Ice Drilling Design and Operations (IDDO) provided drilling support, and the US Antarctic Program provided logistical support for this project. Thanks to Ross Beaudette for lab support at SIO, to Michael Kalk for CO<sub>2</sub> measurements at OSU, and to Monica Arienzo and Nathan Chellman for their heroic operation of the continuous melting system at DRI. The research at University of Bern leading to these results has received funding from the European Research Council (ERC) under the European Union's Seventh Framework Programme FP7/2007-2013 ERC Grant 226172 (ERC Advanced Grant Modern Approaches to Temperature Reconstructions in polar Ice Cores (MATRICs)) and the Swiss national Science Foundation (200020\_172506 (iCEP), 200021\_155906 (NOTICE)). The EDC samples were obtained under the framework of EPICA, a joint European Science Foundation/European Commission scientific program funded by the European Union and national contributions from Belgium, Denmark, France, Germany, Italy, the Netherlands, Norway, Sweden, Switzerland, and the United Kingdom. The main logistic support was provided by IPEV and PNRA at Dome C.

#### Author Contributions

594 J.P.S. and S.S. designed research. S.S., M.H., D.B., and T.K. performed noble gas measurements.  
595 J.A.M., E.J.B., R.H.R., J.R.M. and S.S. performed trace gas field/lab measurements for Taylor  
596 Glacier age model. S.S., D.B., J.A.M., M.N.D., B.B., T.K.B., R.H.R, E.J.B., V.V.P., M.J.R., T.K.,  
597 M.H., J.S., H.F., and J.P.S. analyzed data. S.S. wrote the paper with input from all authors.  
598